UCRL-11160

University of California

Ernest O. Lawrence Radiation Laboratory

EFFECT OF POLYSLIP ON STRAIN-HARDENING IN ALUMINUM SINGLE CRYSTALS

Berkeley, California

DISCLAIMER

UCRL-11160
UC-25 Metals, Ceramics
and Materials
TID-4500 (24th Ed.)

UNIVERSITY OF CALIFORNIA

Lawrence Radiation Laboratory
Berkeley, California

AEC Contract No. W-7405-eng-48

EFFECT OF POLYSLIP ON STRAIN-HARDENING IN ALUMINUM SINGLE CRYSTALS

J. D. Mote

(Ph. D. Thesis)

February 14, 1964

Printed in USA. Price 75 cents. Available from the
Office of Technical Services
U. S. Department of Commerce
Washington 25, D.C.

EFFECT OF POLYSLIP ON STRAIN-HARDENING IN ALUMINUM SINGLE CRYSTALS

Contents

THIS PAGE

WAS INTENTIONALLY

LEFT BLANK

EFFECT OF POLYSLIP ON STRAIN-HARDENING IN ALUMINUM SINGLE CRYSTALS

J. D. Mote

Department of Mineral Technology and
Inorganic Materials Research Division, Lawrence Radiation Laboratory
University of California, Berkeley, California

February 7, 1964

ABSTRACT

Investigations were carried out on the effect of polyslip on strain hardening in fcc single crystals. It is shown that the rate of strain hardening increases for those orientations wherein attractive dislocation intersections occur and that those orientations which produce the greater number of such intersections exhibit the greater strain hardening. It is found that the barrier reactions considered by Hirth are not responsible for any strengthening.

Special experiments on specimens with a $[\bar{1}11]$ tensile axis revealed that the pre-exponential coefficient of the intersection equation is not constant as was previously assumed but varies by several orders of magnitude. Furthermore, at temperatures above the critical temperature, the deformation mechanism is thermally activated.

I. INTRODUCTION

The rate of strain hardening in fcc single crystals increases as the orientation approaches that for duplex slip.[1] Higher rates of strain hardening are attained by crystals oriented respectively for the simultaneous operation of two, four, six, and eight slip systems.[2] No detailed investigations have yet been carried out to rationalize these observations in terms of current theories of dislocation mechanisms.

Previous investigations on the plastic behavior of single crystals of aluminum oriented for single slip and polycrystalline aluminum by Mitra and Dorn[3] revealed that the low-temperature thermally activated mechanism of deformation is that for intersection of forest dislocations by the glissle dislocations as formulated by Seeger.[4] Hence the Seeger equation

$$\dot{\gamma} = NAb\nu e^{-U/kT} \tag{1}$$

applies where

$\dot{\gamma}$ = the shear strain rate

N = the number of points per unit volume where intersection can occur

A = the area swept out per successful intersection

b = the Burgers vector of the dislocation

ν = the Debye frequency

U = the activation energy for intersection

k = Boltzmanns constant

T = the absolute temperature.

The above quantities are assumed to represent suitable smeared average values. In the crude approximation the activation energy for intersection may be written as

$$U = U_o G/G_o - (\tau - \tau_o^* G/G_o)Lb^2 \qquad (2)$$

where

U_o = the activation energy for intersection at absolute zero temperature

G/G_o = the ratio of the shear modulus of elasticity at the test temperature to that at absolute zero

τ = the applied stress

τ_o^* = the internal back stresses at absolute zero, and

L = the average spacing of the forest dislocations.

The source of the internal back stresses is the subject of considerable debate. The purpose of this investigation is to determine the effect of the simultaneous operation of multiple slip systems on the rate of strain hardening in aluminum single crystals and the influence of orientation on the buildup of back stresses during deformation.

II. EXPERIMENTAL TECHNIQUE

Single crystal specimens of high purity Al (99.995 atomic percent) were produced in the following manner:

(1) Single crystal spheres of approximately 1 in. diam. were grown in graphite crucibles under argon by the modified Bridgman technique.

(2) The orientation of the spheres was determined by the Laue back-reflection technique.

(3) The spheres were so oriented in graphite crucibles containing a 3/8-in. diam cylindrical cavity above the spherical receptical to give, respectively, [001], [011], [$\bar{1}$11], and [$\bar{1}$12] directions along the cylinder axis. Another sphere

was so oriented as to give an angle of 45° between the <111> and the cylinder axis as well as 45° between the <110> and the cylinder axis. Oriented cylindrical single crystals were produced by placing a polycrystalline rod above the spherical seed, melting partially into the sphere under argon, and growing an oriented rod from the spherical seed.

(4) Finally, oriented single crystal rods approximately 4-1/2 in. in length were grown using sections of the above described rod as seeds.

(5) A reduced gage section approximately 2 in. in length and 0.225 in. in diameter was produced by spark machining. The spark damaged layer was removed by etching away 0.002 in. from the diameter.

(6) The specimens were annealed at about 823°K in a salt bath for approximately 1/2 h prior to testing.

Tension experiments were carried out in an Instron tensile testing machine over the temperature range 4.2° to 370°K.

III. EXPERIMENTAL PROCEDURE AND RESULTS

In order to determine the effect of the orientation on the rate of strain hardening, experiments were carried out at 77°K in an Instron tensile testing machine for variously oriented single crystals at a cross-head speed of 0.02 in./min. Table I summarizes the orientations tested and the number of slip systems operative in each case. The diagram of critical resolved shear stress vs shear strain is shown in Fig. 1. The method of calculating the resolved shear strain is given in the Appendix. In order to obtain data for calculating the apparent activation volume,

which is defined $v = Lb^2$ in the Seeger model, values of β defined by

$$\beta = \frac{\partial \ell n \gamma}{\partial \tau} \approx \left(\frac{\ell n \dot{\gamma}_2 / \dot{\gamma}_1}{(\tau_2 - \tau_1)} \right)_T \tag{3}$$

were obtained by means of a quick gear shift change which reduced the crosshead speed by a factor of ten. These results are shown in Fig. 2. Figure 1 reveals that the rate of strain hardening increases as the number of participating slip systems increase except in the case of the [012] orientation which exhibits the lowest rate of strain hardening. Figure 2 shows that the apparent activation volume at a given strain decreases as the number of participating slip systems increase.

In order to determine the nature of the variation of back stresses these additional experiments were conducted. Specimens with the tensile axis along the [111] direction were selected for these experiments since they exhibited a high rate of strain hardening but did not exhibit the instability which was observed for some specimens oriented with the tensile axis along the [001] axis. Since a strain hardened state of a material may be defined by the flow stress τ_p at a particular strain rate and temperature, states a, b, c, and d defined by the flow stress τ_p at 370°K and a strain rate of 1.0×10^{-5} sec^{-1} were selected. Specimens described above were first prestrained to the lowest state, a, and subsequently deformed at a selected strain rate and temperature, returned to 370°K, prestrained to state b, and again deformed at the selected temperature and strain rate, etc. The deformation at the selected temperature and strain rate was always small so as to minimize the changes in the structure that could result due to the different experimental conditions. The results of a series of experiments conducted at strain rates of 1.0×10^{-3} sec^{-1} and 1.0×10^{-5} sec^{-1} over the temperature range 4.2° to 390°K are recorded

in Fig. 3. These results indicate that the flow stress decreases linearly with increasing temperature at constant strain rate over Region I and decreases less rapidly with increasing temperature over Region II.

IV. ANALYSIS OF RESULTS AND DISCUSSION

The intersection theory assumes that the strain hardened state is described in terms of the variables τ_o^*, L, and NA. Previous analyses of the intersection mechanism have assumed that NA does not vary materially during strain hardening. However, until recently no experimental results were available which would allow one to make judgment on the validity of this assumption. The experimental results represented in Fig. 3, however, allow a calculation of NA to be made.

Over Region I the results can be analyzed in terms of the Seeger equation for intersection, namely

$$\dot{\gamma} = NAb\nu e^{-\frac{U_o G/G_o - (\tau - \tau_o^* G/G_o)Lb^2}{kT}} \tag{4}$$

when $T < T_c$. Rewriting Eq. 4 in the form

$$\tau G_o/G = U_o/Lb^2 + \tau_o^* - kTG_o/Lb^2 G \ell n(NAb\nu/\dot{\gamma}) \tag{5}$$

when $T < T_c$ reveals that $\tau G_o/G$ decreases linearly with TG_o/G at constant strain rate since for a given strain hardened state U_o, L, τ_o^*, and NA are constant. The excellent agreement of the experimental results with the dictates of Eq. 6 is shown in Figs. 3 and 4. For a given strain hardened state at a constant strain rate the slope of the curve is

$$B_{\dot{\gamma}_1} = k/Lb^2 \ell n (NAb\nu/\dot{\gamma}_1) \tag{6}$$

hence the ratio of the slopes for two different strain rates gives

$$B_{\dot{\gamma}_1}/B_{\dot{\gamma}_2} = \frac{\ell n(NAb\nu/\dot{\gamma}_1)}{\ell n(NAb\nu/\dot{\gamma}_2)} \quad . \tag{7}$$

Solving for $NAb\nu$ one obtains

$$\ell nNab\nu = \frac{B_{\dot{\gamma}_1}/B_{\dot{\gamma}_2}(\ell n\dot{\gamma}_2) - (\ell n\dot{\gamma}_1)}{B_{\dot{\gamma}_1}/B_{\dot{\gamma}_2} - 1} \quad . \tag{8}$$

The variation of $\ell nNab\nu$ for various states characterized by the stress τ_p at 370°K and a strain rate of 1.0×10^{-5} sec^{-1} is given in Fig. 5. Table II gives the values of NA for various strain-hardened states. This table reveals that, contrary to the assumptions which have been made in the past, NA is not constant but varies by several orders of magnitude. It should be pointed out, however, that NA can scatter quite widely about the reported values for the following reason: The effect of strain rate on the flow stress is small, therefore, the slopes of the two lines for a given state at two different strain rates are not vastly different even though the strain rates differ by a factor of 100. Examination of Eq. 9 reveals that a small error in the ratio $B_{\dot{\gamma}_1}/B_{\dot{\gamma}_2}$, which has a value near 1, can cause a considerable change in the value of NA. Nevertheless it is difficult to believe that the trend shown in Fig. 5 can be explained away by experimental scatter. Using the same experimental technique, Rosen, Nunes, and Dorn[5] have found similar trends in polycrystalline aluminum. The reason for such a dramatic change in NA is not clear. However, one possibility which admits such variation may be as follows. Although a one to one correspondence between the observations of electron microscopy and the dictates of intersection theory cannot be expected since the quantities NA and L represent smeared average values the following results seem to be pertinent. It has been observed that during the deformation of aluminum[6]

and other fcc metals[7,8] that a cell structure is formed wherein the cell walls are composed of dense dislocation tangles while the cell interior is relatively dislocation free. The density of dislocations in heavily deformed aluminum has been reported as 10^{10} cm^{-2} (9) and for copper the dislocation density in the tangles at the end of stage II has been found to be as high as 5×10^{11} cm^{-2}, (10) furthermore during deformation the cell size decreases to approximately one-half its original diameter.[11] If, as in the case of the simple theory, N is associated with the cube of the dislocation density, but A is associated with some average area which depends on the cell area it is clearly seen that while A decreases only by a small factor the density of dislocations in the entanglements increases by several orders of magnitude, hence a great increase in the product NA is possible.

Having established the values of $\ell nNAb\nu$ one can calculate the activation volume for the various strain hardened states from the relation

$$v = Lb^2 = k/B_{\gamma_1} \ell nNAb\nu \qquad (9)$$

These results are shown in Fig. 6. The activation volume can be obtained from the data of Fig. 2 since differentiation of Eq. 4 with respect to the stress gives

$$\partial \ell n \gamma / \partial \tau = Lb^2/kT \approx \beta \qquad (10)$$

hence

$$\beta kT \simeq Lb^2 = v \qquad (11)$$

The activation volumes obtained by the change in strain rate technique are plotted for comparative purposes. The activation volumes obtained by the two techniques are in reasonable agreement. The differences that

exist may be due to a different structure being developed when straining takes place exclusively at 370°K. This is in harmony with the electron microscope observation[7] that a smaller cell size is developed when deformation is executed at lower temperatures.

Values of the activation volume for polycrystalline aluminum[3] at 90°K are also recorded. The close agreement of these values with those obtained at 77°K for a single crystal with a $[\bar{1}11]$ tensile axis attests to the validity of the suggestion by Kochs[2] that the appropriate single crystal stress-strain curve to predict polycrystalline behavior is that for which polyslip occurs.

Figure 3 indicates that at the lowest strain hardened state over Region II there is only a slight decrease of $\tau G_o/G$ with increasing temperature. Examination of Eq. 5 reveals that thermal fluctuation assists only in overcoming U_o. Hence, this equation applies only when $U_o > kTG_o/G\ell n(NAb\nu/\dot{\gamma})$. For temperatures where $U_o < kTG_o/G\ell n(NAb\nu/\dot{\gamma})$ successful thermal fluctuations are immediate and in this range

$$\tau G_o/G = \tau_o^* \tag{12}$$

when $T > T_c$. Above about 200°K for state (a) the corrected flow stress, $\tau G_o/G$ is almost constant with increasing temperature, therefore, Eq. 12 applies, and the value of τ_o^* for state (a) is established. Having determined the value of τ_o^* for state (a) and observing that for $T = 0$

$$\tau_o G_o/G = U_o/Lb^2 + \tau_o^* \tag{13}$$

one can calculate U_o and obtain $U_o = 4,400$ cal/mole. This value for the activation energy is in reasonable agreement with that of 4 700 cal/mole obtained by Rosen, Nunes, and Dorn[5] for polycrystalline Al.

Knowing the value of U_o one can now calculate the values of τ_o^* for states (b), (c), and (d). The results are shown in Fig. 7 with the results of Rosen, Nunes, and Dorn.[5] As in the case of the activation volume the variation of τ_o^* for single crystals with a $[\bar{1}11]$ tensile axis and polycrystals is in good agreement. At the higher strain hardened states at temperatures above T_c (in Region II) there is a significant decrease in flow stress with increasing temperature. Hence the mechanism of deformation in Region II is thermally activated and may be controlled by a dynamic recovery process.

The results of Fig. 1 clearly show the effect of the orientation on work-hardening in aluminum. Except for the [012] orientation which has two operative slip systems, the rate of work hardening increases as the number of operative slip systems increases. The reason for the low rates of work hardening for the [012] orientation will be discussed later. In harmony with the observed increase of work hardening the activation volume decreases more rapidly with strain as the number of operative slip systems increases as shown in Fig. 8. Equation 5 reveals that a decrease in the activation volume can partially account for the work hardening that is observed. However, since as discussed previously $NAb\nu$ is not constant, these results cannot be used to determine the variation of the back stress with deformation by the techniques previously employed.[3] Nevertheless, some comparisons can be made.

There are 24 different Burgers vectors of the type $a/2\langle 110\rangle$ in the fcc lattice if one considers both positive and negative directions. Hirth[12] considers the possible reactions of the primary dislocations in the fcc lattice with secondary dislocations and concludes that there are three important barriers of the type considered by Cottrell[13] and Lomer.[14] The three barrier dislocation reactions are

$$a/6\,[2\bar{1}\bar{1}] + a/6\,[1\bar{2}1] + a/6\,[121] + a/6\,[\bar{1}12] \longrightarrow a/6\,[\bar{1}21] + a/6\,[121] + a/6\,[101] \tag{14}$$

which is the original Cottrell-Lomer reaction and will be referred to herein as a Cottrell-Lomer barrier;

$$a/6\,[2\bar{1}\bar{1}] + a/6\,[12\bar{1}] + a/6\,[121] + a/6\,[21\bar{1}] \longrightarrow a/6\,[2\bar{1}\bar{1}] + a/6\,[21\bar{1}] + a/6\,[202] \tag{15}$$

referred to herein as a Hirth I barrier; and

$$a/6\,[2\bar{1}\bar{1}] + a/6\,[1\bar{2}1] + a/6\,[\bar{2}11] + a/6\,[\bar{1}\bar{2}\bar{1}] \longrightarrow a/6\,[1\bar{2}1] + a/6\,[\bar{1}\bar{2}\bar{1}] + a/6\,[0\bar{2}0] \tag{16}$$

referred to herein as a Hirth II barrier, where a is the lattice parameter. By consideration of second order, short range interactions Hirth concludes that the reactions given by Eqs. 15 and 16 represent stronger barriers to glide than the barrier represented by Eq. 14. In addition, there are certain other reactions which are not favorable since the resultant dislocations have a greater energy than the sum of the energies of the reacting dislocations and therefore repel each other, still other reactions cause annihilation and some produce new glide dislocations.

The only difference in the specimens, whose stress-strain curves are recorded in Fig. 1, is the orientation and therefore the number of operative slip systems. Hence, it is reasonable to assume that the only important dislocation interactions or reactions contributing to the buildup of back stresses occurs between the moving dislocations and the dislocations originally present play only a minor role. Assuming that the reactions important to hardening occur only by the combination of gliding dislocations, one can determine the number of various kinds of reactions or interactions for pairs of dislocations for the various orientations. Table III lists the

slip systems which have equal maximum shear stresses for each orientation. Table IV summarizes the number of various kinds of reactions for each orientation and Table V gives an example of each type of reaction. Only reactions between pairs of dislocations lying in different glide planes are considered since no important barrier forming reactions occur between dislocations lying in the same glide plane.

Table IV clearly reveals that the Hirth I barrier and Hirth II barrier are not responsible for hardening since they are the only barriers formed for the [012] orientation and this represents the orientation for which the rate of strain hardening is the lowest, the extent of "easy glide" being greater than that for single slip. Qualitatively the formation of Cottrell-Lomer barriers is in harmony with the experimental observations. However, no evidence of the existence of these barriers has been observed in aluminum.[8] On the contrary, as discussed previously, a cell structure is formed bounded by dense dislocation tangles. Hence Cottrell-Lomer barriers as the source hardening remains questionable. As will be shown subsequently, the results are in complete harmony with the conclusions of Saada[15] that hardening occurs because of the attractive junctions of intersecting dislocations. It is suggested here, however, that the major source of these junctions is due to intersections of moving dislocations with other moving dislocations. Hirsch[16] pointed out that intersecting dislocations in structures such as fcc interact with one another when their slip planes are not mutually perpendicular. The problem is made more complicated by the fact that the dislocations can attract or repel depending on the mutual orientation of the dislocations and their Burgers vectors. This problem has been studied in considerable detail by Saada.

Saada[17] considered two dislocations A and B and as they come into contact they form an unstable quadruple node. If the scalar product of the Burgers vectors of the dislocations A and B is negative the quadruple node can decompose into a third dislocation C (Fig. 9) with Burgers vector b_3 but if the scalar product is positive the junction is repulsive. The decomposition of the quadruple node in the attractive case stabilizes the structure hence it is more difficult for dislocations to cross at attractive junctions than at repulsive ones. Indeed Saada shows that the hardening due to attractive junctions predominates that due to repulsive ones. The stresses necessary to cause dislocations to cross at attractive junctions are practically temperature independent whereas the repulsive junctions cause a temperature dependent hardening since such crossings can be thermally activated.

Table VI summarizes the number of attractive junctions formed by dislocation intersection for the various tension axis orientations. Due to the nature of the intersecting dislocations certain of these nodes will form parallel to the $\{001\}$ planes whereas others will form parallel to the $\{111\}$ planes, hence this distinction has been made in the table.

Table VI clearly reveals that hardening due to the formation of attractive nodes is in harmony with experimental results recorded in Fig. 1. Furthermore, for the $[\bar{1}11]$ and [001] orientations segments should form parallel to the $\{001\}$ and $\{111\}$ planes hence this may account for the electron microscopy observations that the dislocations tangles forming the cell wall in deformed aluminum tend to lie parallel to the $\{001\}$ and $\{111\}$ planes.[8] Systematic study of the deformed structure as a function of orientation via electron microscopy should prove very enlightening. One additional orientation that should be included in future

studies is that for the simultaneous operation of two slip systems having the same glide plane. Such an orientation should also reveal a very low rate of work hardening because no important barrier reactions occur in this case.

V. CONCLUSIONS

It is concluded that:

(1) The pre-exponential coefficient of the Seeger equation for intersection is not constant during deformation as has previously been assumed but changes by several orders of magnitude.

(2) Deformation in the region above the critical temperature defined by the Seeger equation is also thermally activated.

(3) The activation volume decreases more rapidly with deformation as the number operative slip systems increase.

(4) The rate of hardening is in harmony with the formation of stable nodes at attractive dislocation intersections.

(5) The barriers considered by Hirth to form strong obstacles to slip are shown to be ineffective.

ACKNOWLEDGMENTS

I am indebted to Professor John E. Dorn who suggested the problem and who was a source of inspiration throughout its execution. Dr. S.K. Mitra is thanked for his contributions during some of the early experimental phases of this work. The discussions with Dr. A. Rosen, Professor F.E. Hauser, and Messrs. A. Nunes and A. Amadieh were most helpful in clarifying many issues. Dr. A. Mukherjee is especially thanked for assistance during the latter experimental phases and for many helpful discussions. Messrs. G. Chao, R. Walson, P. Nishikawa, and E. Garlinger helped measurable with the careful specimen preparation and data reduction. Finally, I owe a great debt to my wife Blanche without whose patience and understanding this work could never have been completed.

This work was performed under the auspices of the U.S. Atomic Energy Commission.

Table I. Orientation and number of operative slip systems.

Orientation of tensile axis	Number of operative slip systems
45° to $[10\bar{1}]$ and (111)	1
[012]	2
$[\bar{1}12]$	2
[011]	4
$[\bar{1}11]$	6
[001]	8

Table II. Variation of NAbν with state.

State	$\tau_p G_o/G \times 10^{-7}$ dynes/cm^2	NAbν sec^{-1}
a	4.81	2.0×10^3
b	7.82	2.3×10^5
c	10.69	5.8×10^7
d	13.89	7.6×10^8

Table III. Operative slip systems for various orientations.

Orientation of tensile axis	Slip systems
45° to (111) and $[\bar{1}01]$	$(111)[\bar{1}01]$
[012]	$(111)[10\bar{1}]$, $(111)[\bar{1}01]$, $(\bar{1}11)[101]$, $(\bar{1}11)[\bar{1}0\bar{1}]$
$[\bar{1}12]$	$(111)[10\bar{1}]$, $(111)[\bar{1}01]$, $(11\bar{1})[011]$, $(11\bar{1})[0\bar{1}\bar{1}]$
[011]	$(111)[1\bar{1}0]$, $(111)[\bar{1}10]$, $(111)[10\bar{1}]$, $(111)[\bar{1}01]$ $(\bar{1}11)[110]$, $(\bar{1}11)[\bar{1}\bar{1}0]$, $(\bar{1}11)[101]$, $(\bar{1}11)[\bar{1}0\bar{1}]$
$[\bar{1}11]$	$(111)[\bar{1}10]$, $(111)[1\bar{1}0]$, $(111)[10\bar{1}]$, $(111)[\bar{1}01]$ $(1\bar{1}1)[\bar{1}01]$, $(1\bar{1}1)[10\bar{1}]$, $(1\bar{1}1)[011]$, $(1\bar{1}1)[0\bar{1}\bar{1}]$ $(11\bar{1})[1\bar{1}0]$, $(11\bar{1})[\bar{1}10]$, $(11\bar{1})[011]$, $(11\bar{1})[0\bar{1}\bar{1}]$
[001]	$(111)[10\bar{1}]$, $(111)[\bar{1}01]$, $(111)[01\bar{1}]$, $(111)[0\bar{1}1]$ $(\bar{1}11)[101]$, $(\bar{1}11)[\bar{1}0\bar{1}]$, $(\bar{1}11)[01\bar{1}]$, $(\bar{1}11)[0\bar{1}1]$ $(1\bar{1}1)[10\bar{1}]$, $(1\bar{1}1)[\bar{1}01]$, $(1\bar{1}1)[011]$, $(1\bar{1}1)[0\bar{1}\bar{1}]$ $(11\bar{1})[101]$, $(11\bar{1})[\bar{1}0\bar{1}]$, $(11\bar{1})[011]$, $(11\bar{1})[0\bar{1}\bar{1}]$

Table IV. Summary of the number of various dislocation reactions for the indicated orientations.

Resultant dislocation	Orientation of tensile axis					
	45° to [101] and (111)	[012]	[$\bar{1}$12]	[110]	[$\bar{1}$11]	[001]
Cottrell-Lomer barrier	0	0	2	4	6	8
Hirth I barrier	0	2	0	4	0	16
Hirth II barrier	0	2	0	4	0	16
No reaction, i.e., "repulsion"	0	0	2	4	24	32
Annihilation	0	0	0	0	6	8
Glide dislocation	0	0	0	0	12	16

Table V. Typical reactions for each of the resultant dislocations.

Resultant dislocation	Reacting dislocations		Burgers vector of resultant dislocations	Line of intersection of glide plane	Glide plane of resultant dislocation
Cottrell-Lomer barrier	$[10\bar{1}]_{(111)}$	$[011]_{(11\bar{1})}$	a/2 [110]	$[1\bar{1}0]$	(001)
Hirth I barrier	$[10\bar{1}]_{(111)}$	$[101]_{(11\bar{1})}$	a/2 [200]	$[1\bar{1}0]$	(001)
Hirth II barrier	$[10\bar{1}]_{(111)}$	$[\bar{1}0\bar{1}]_{(11\bar{1})}$	a/2 [00$\bar{2}$]	$[1\bar{1}0]$	(110)
No reaction	$[10\bar{1}]_{(111)}$	$[0\bar{1}\bar{1}]_{(1\bar{1}1)}$	a/2 [1$\bar{1}\bar{2}$]	--	--
Annihilation	$[\bar{1}01]_{(111)}$	$[10\bar{1}]_{(1\bar{1}1)}$	a/2 [000]	--	--
Glide dislocation	$[\bar{1}01]_{(111)}$	$[01\bar{1}]_{(\bar{1}11)}$	a/2 [$\bar{1}$10]	$[01\bar{1}]$	(111)

Table VI. Attractive junctions formed for the various orientations.

	45° to {111} and <110>	[012]	[112]	[011]	[111]	[001]
Segments parallel to (001)	0	0	2	4	6	8
Segments parallel to (111)	0	0	0	0	12	16

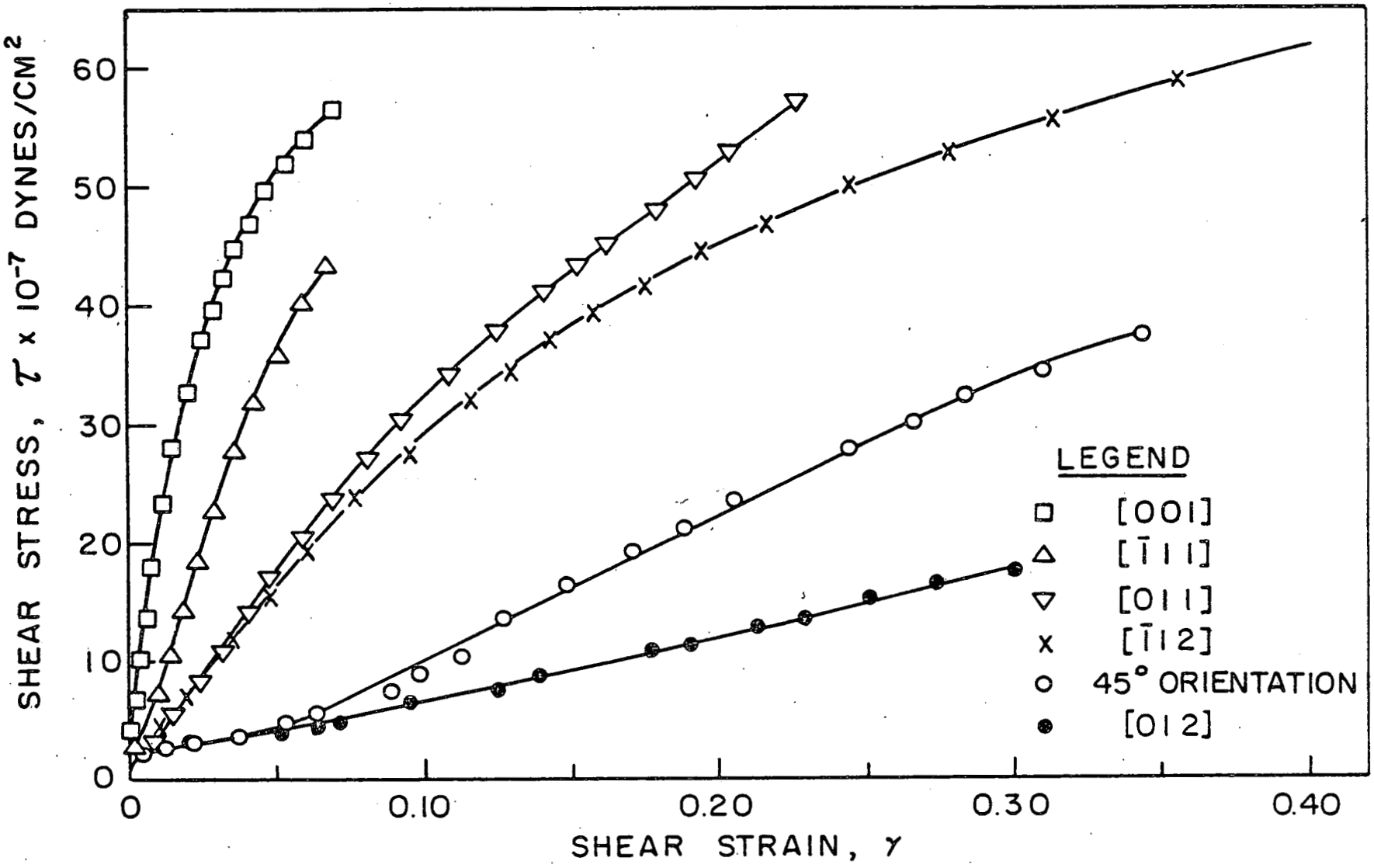

FIG. 1. STRESS STRAIN CURVES FOR VARIOUS ORIENTATIONS

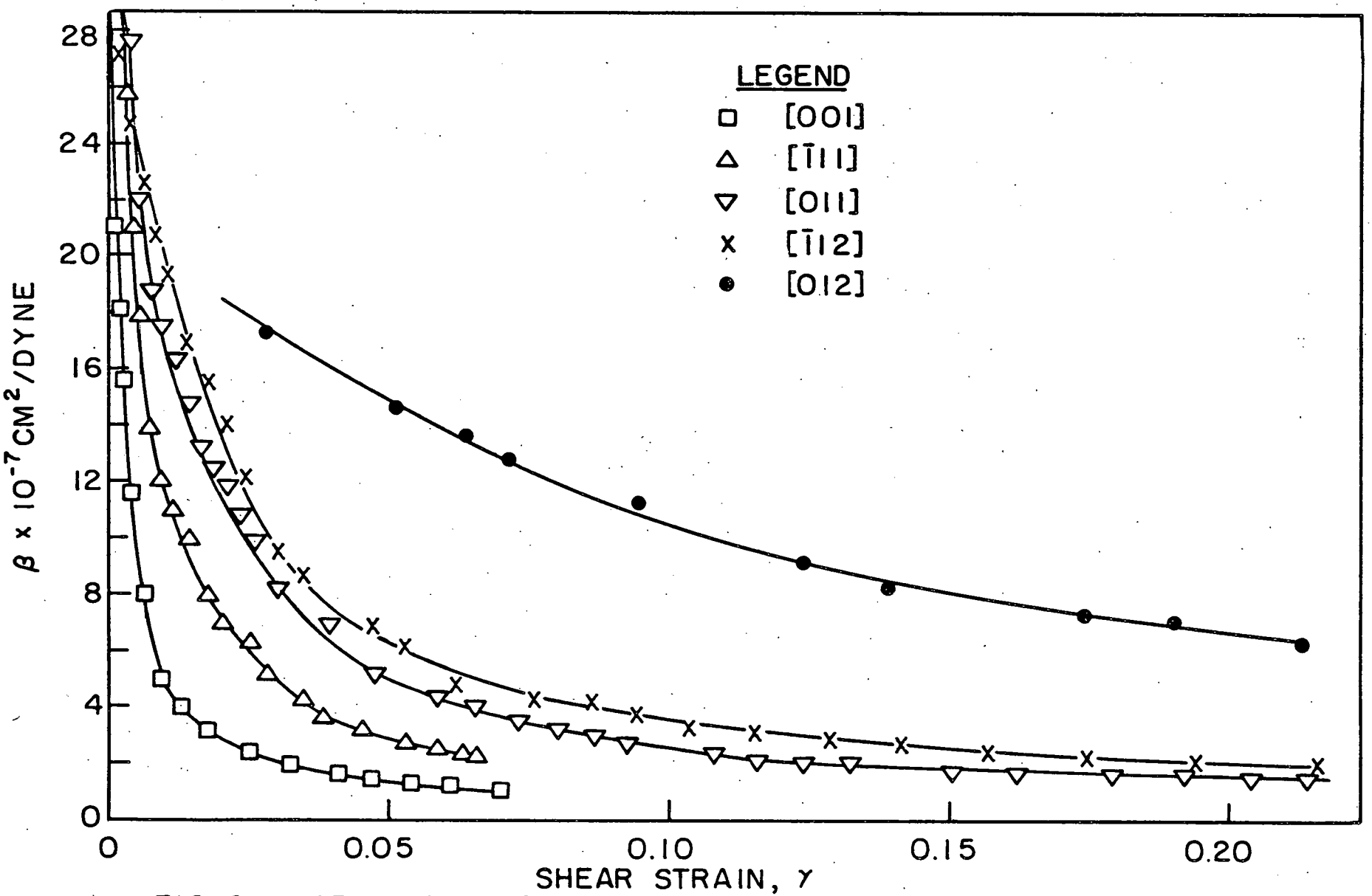

FIG. 2. VARIATION OF β vs. STRAIN FOR VARIOUS ORIENTATIONS.

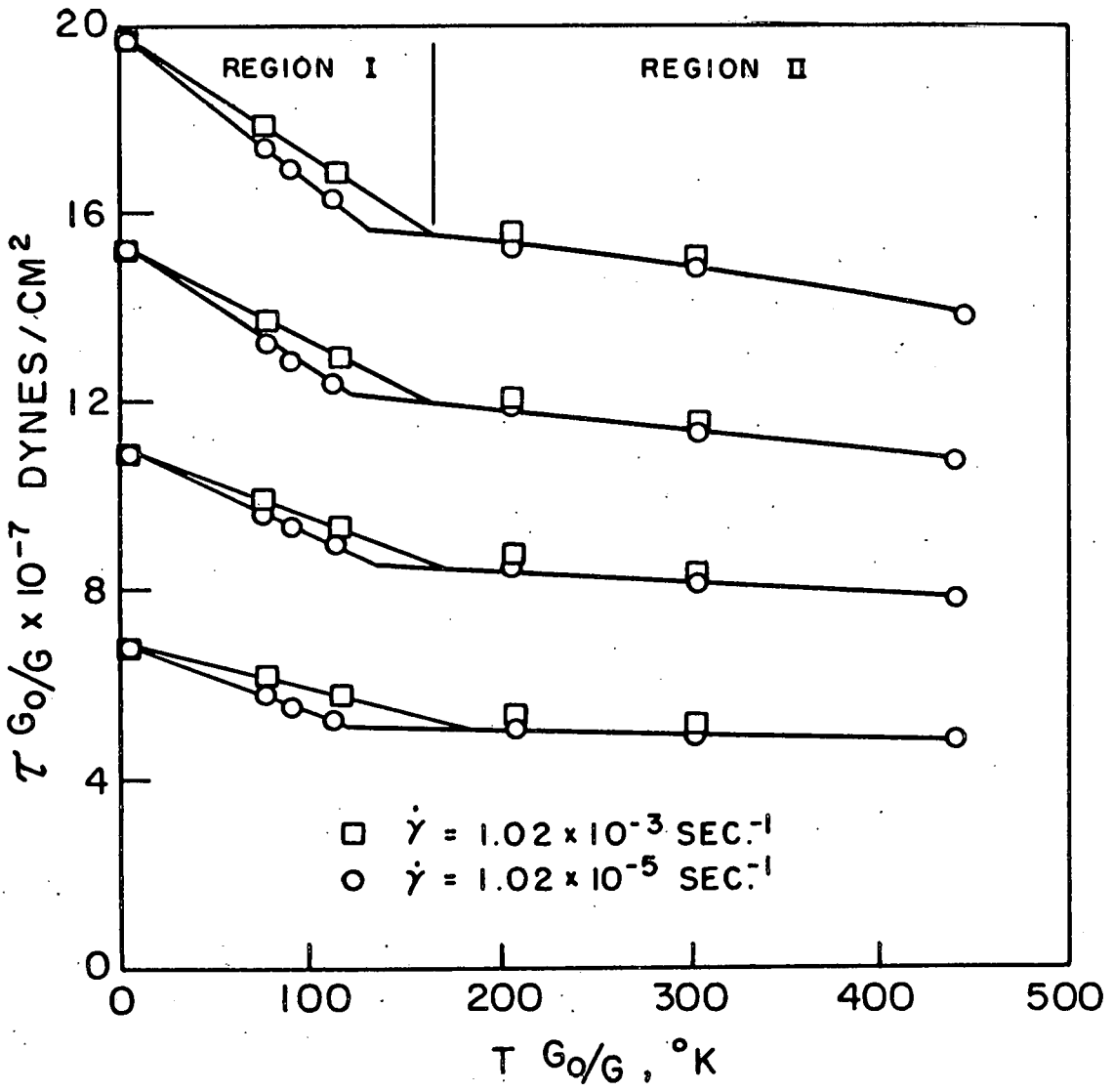

FIG. 3. EFFECT OF TEMPERATURE ON THE FLOW STRESS.

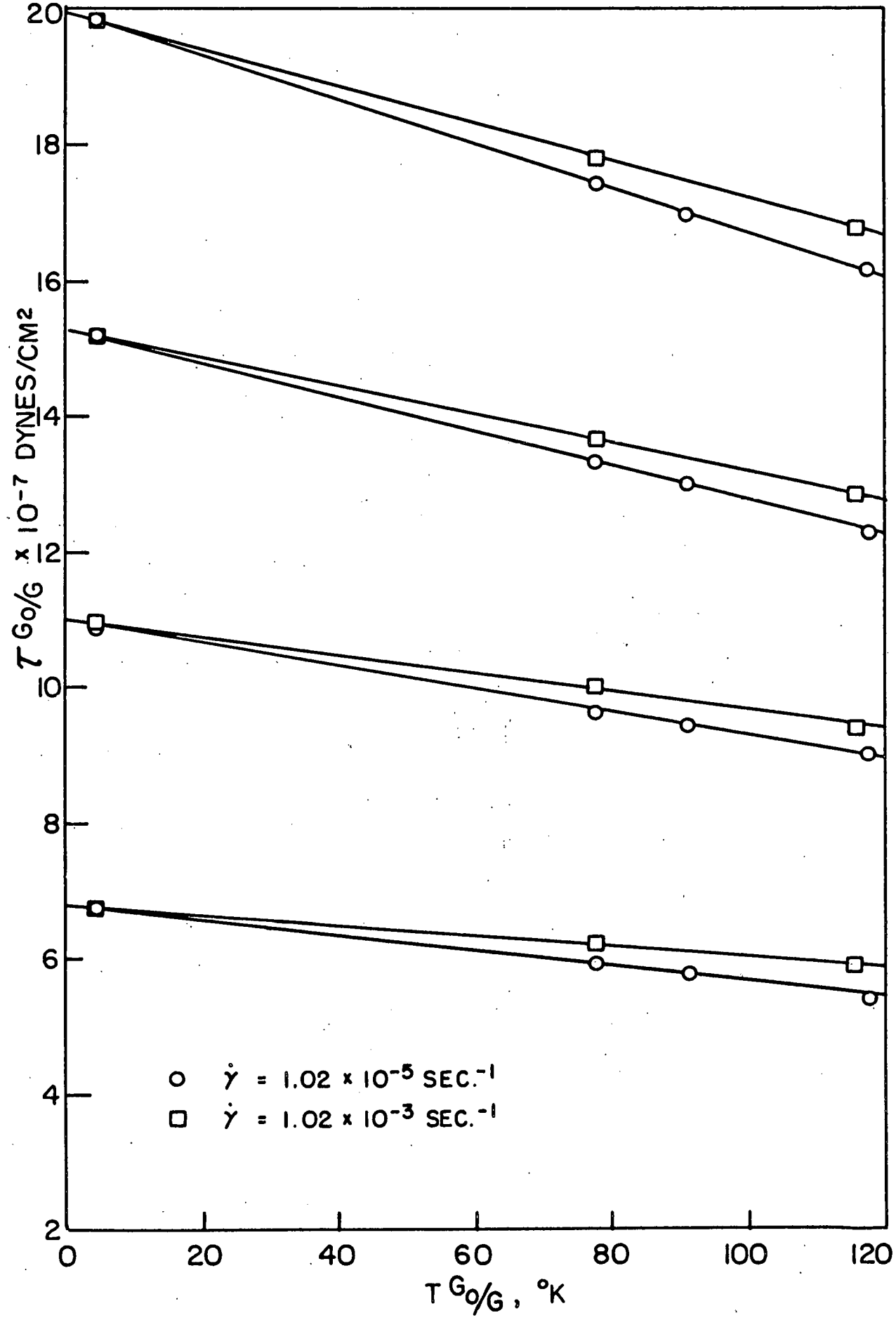

FIG. 4. EFFECT OF TEMPERATURE ON THE FLOW STRESS.

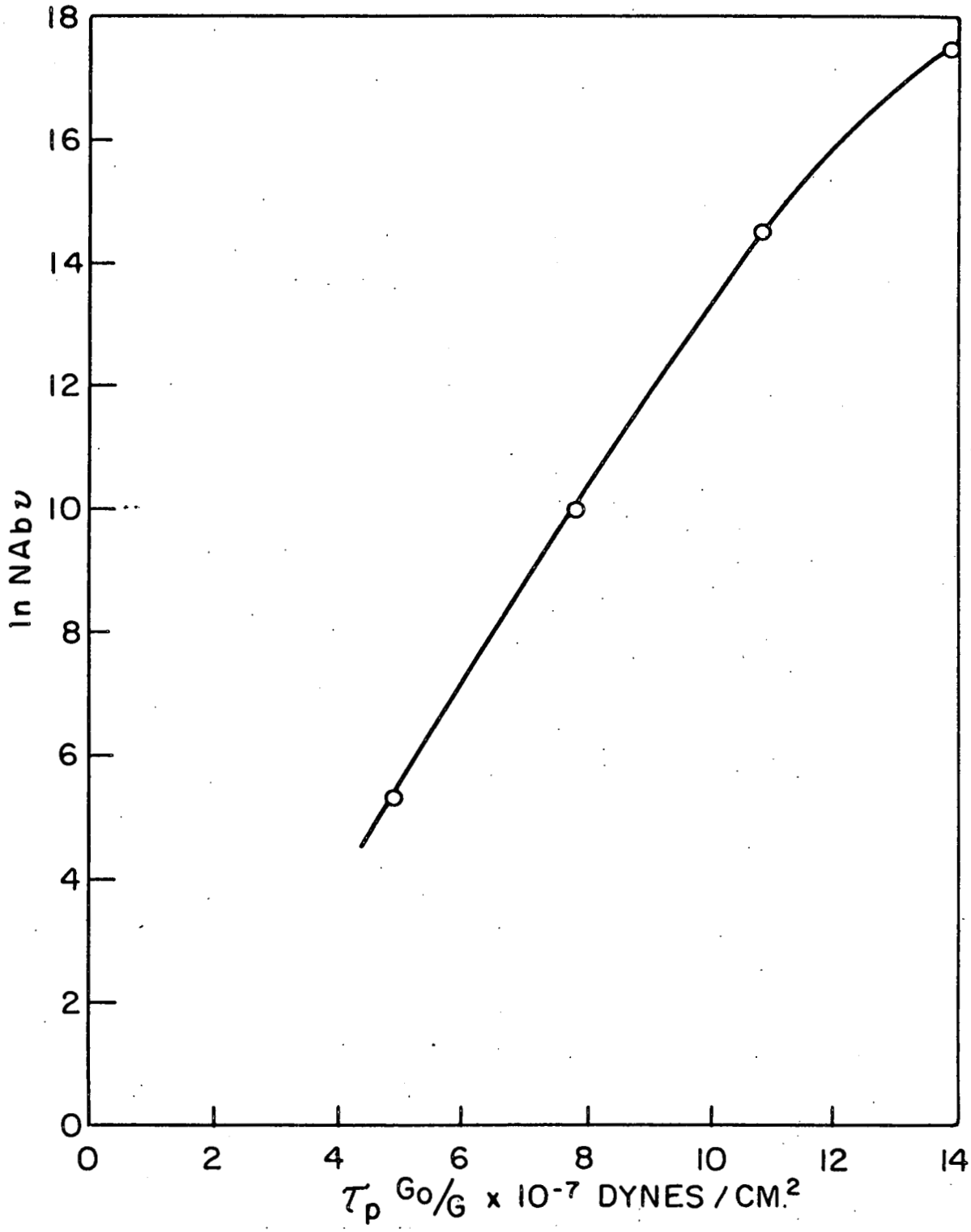

FIG. 5. VARIATION OF ln NAbν WITH PRESTRESS.

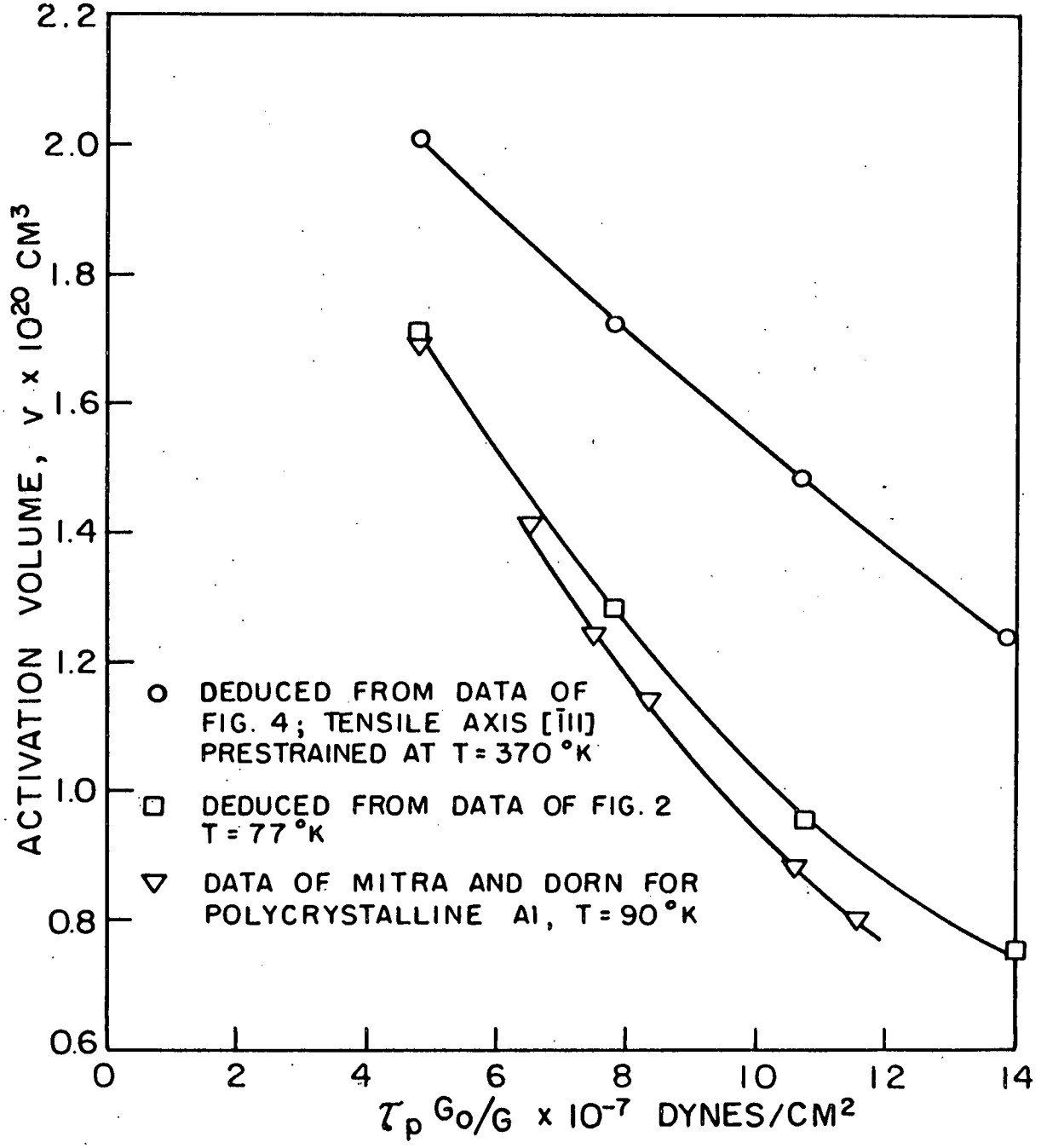

FIG. 6. CHANGE OF ACTIVATION VOLUME WITH STRAIN HARDENING.

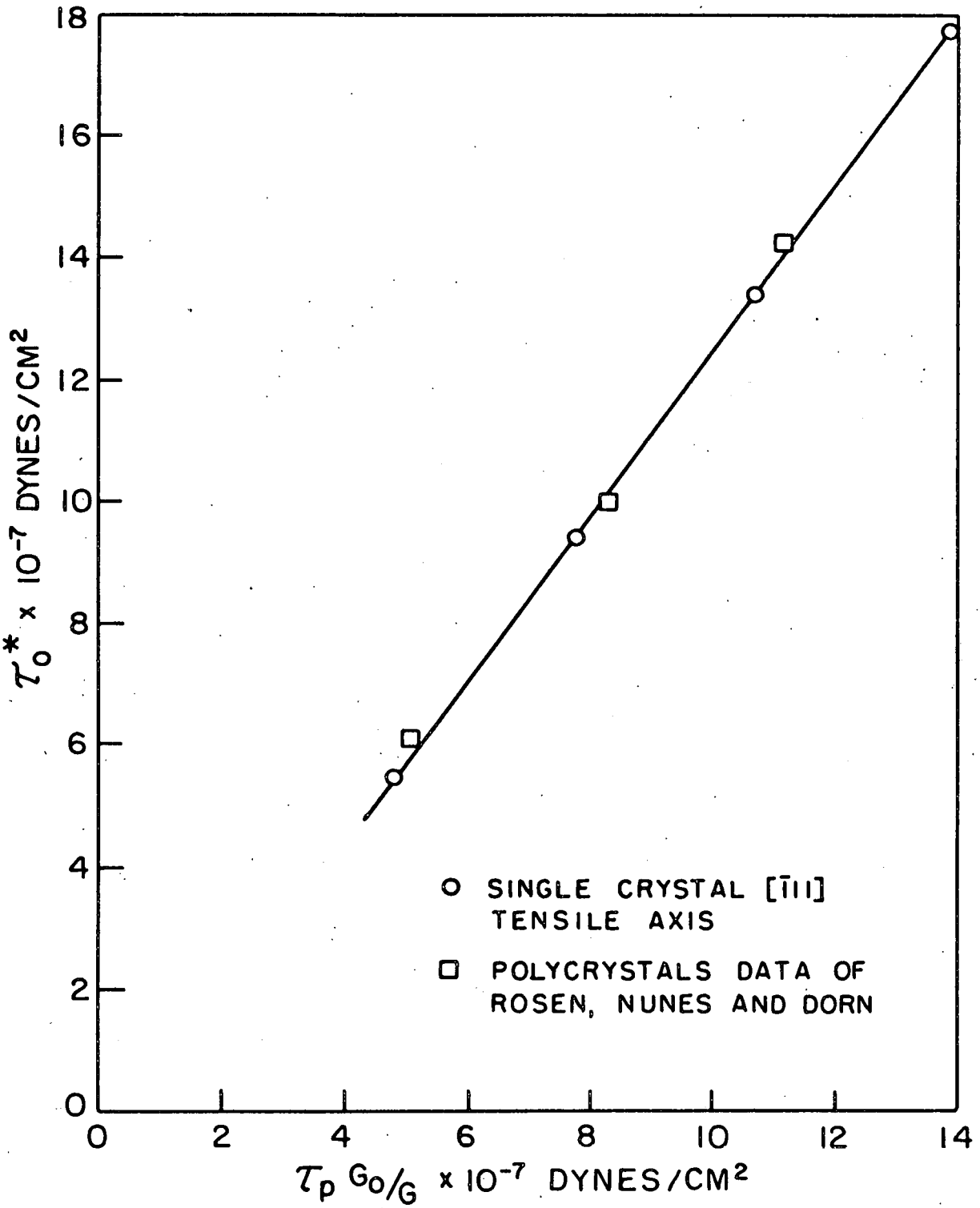

FIG. 7. CHANGE OF BACK STRESS WITH PRESTRESS.

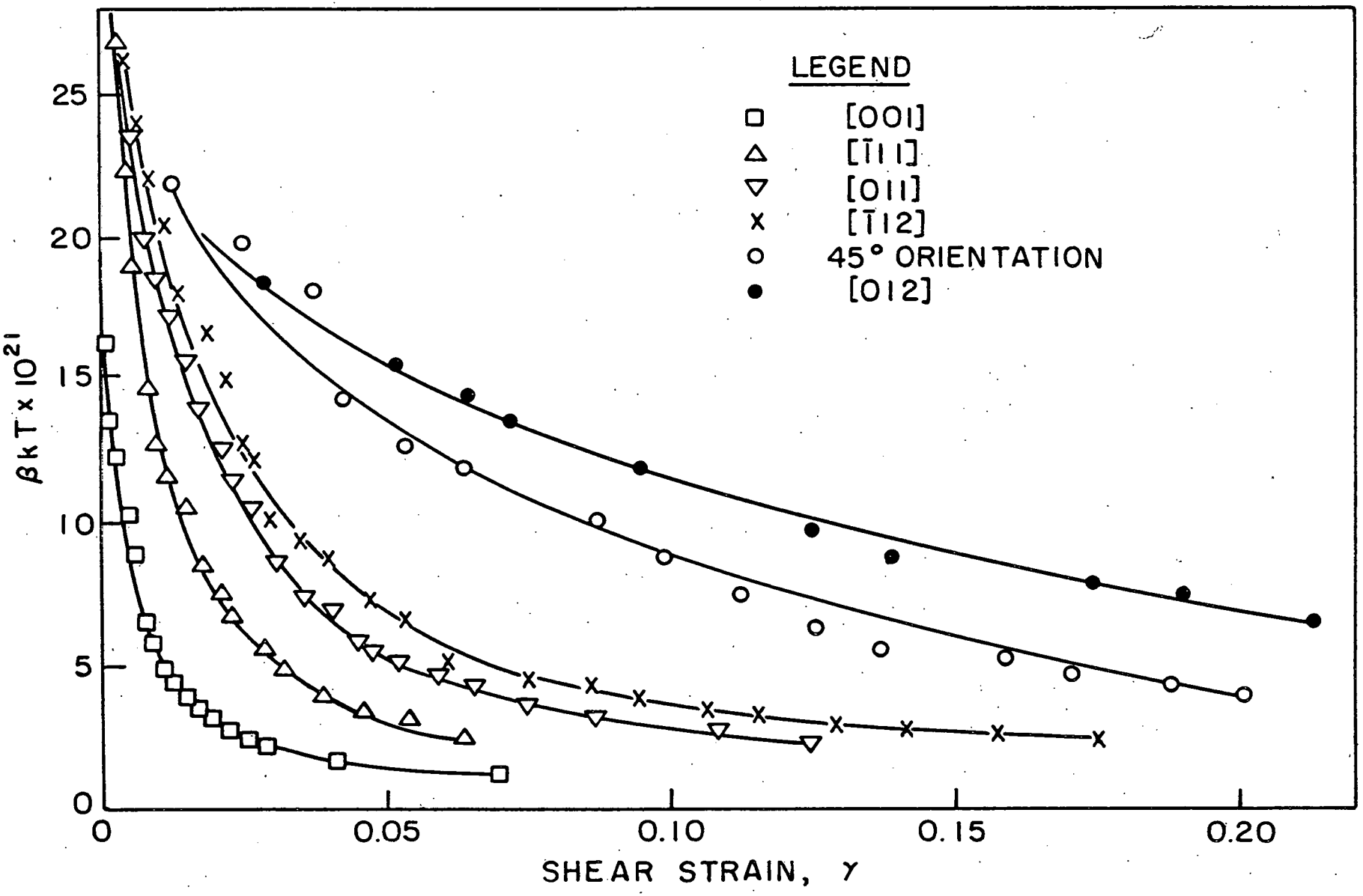

FIG. 8. ACTIVATION VOLUME vs. SHEAR STRAIN.

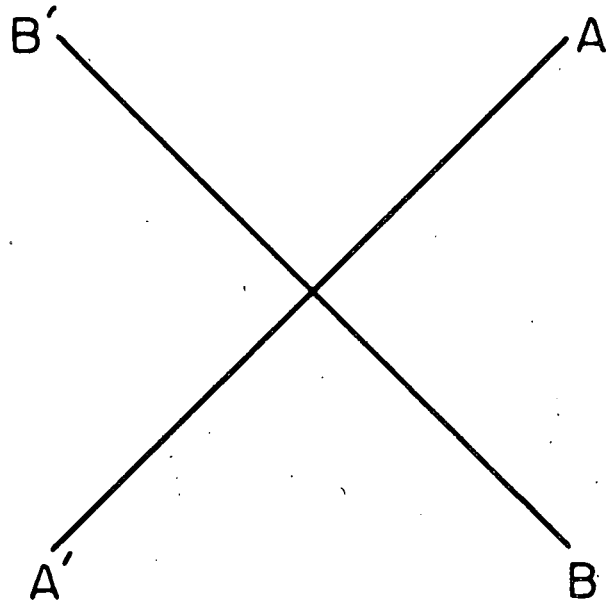

(a) BEFORE INTERSECTION.

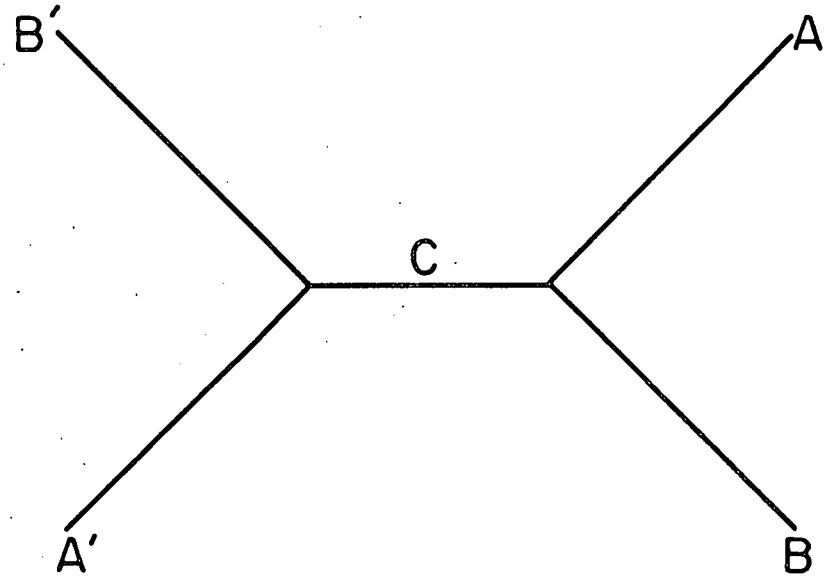

(b) CONFIGURATION AFTER INTERSECTION.

FIG. 9. INTERSECTION OF ATTRACTIVE DISLOCATIONS.

This report was prepared as an account of Government sponsored work. Neither the United States, nor the Commission, nor any person acting on behalf of the Commission:

A. Makes any warranty or representation, expressed or implied, with respect to the accuracy, completeness, or usefulness of the information contained in this report, or that the use of any information, apparatus, method, or process disclosed in this report may not infringe privately owned rights; or

B. Assumes any liabilities with respect to the use of, or for damages resulting from the use of any information, apparatus, method, or process disclosed in this report.

As used in the above, "person acting on behalf of the Commission" includes any employee or contractor of the Commission, or employee of such contractor, to the extent that such employee or contractor of the Commission, or employee of such contractor prepares, disseminates, or provides access to, any information pursuant to his employment or contract with the Commission, or his employment with such contractor.